Fig. 9.6. Schematic molecular orbital diagrams: (*a*) O_2; (*b*) CO. The $C_{\infty v}$ symmetry labelling appropriate to a heteronuclear system is used for both molecules.

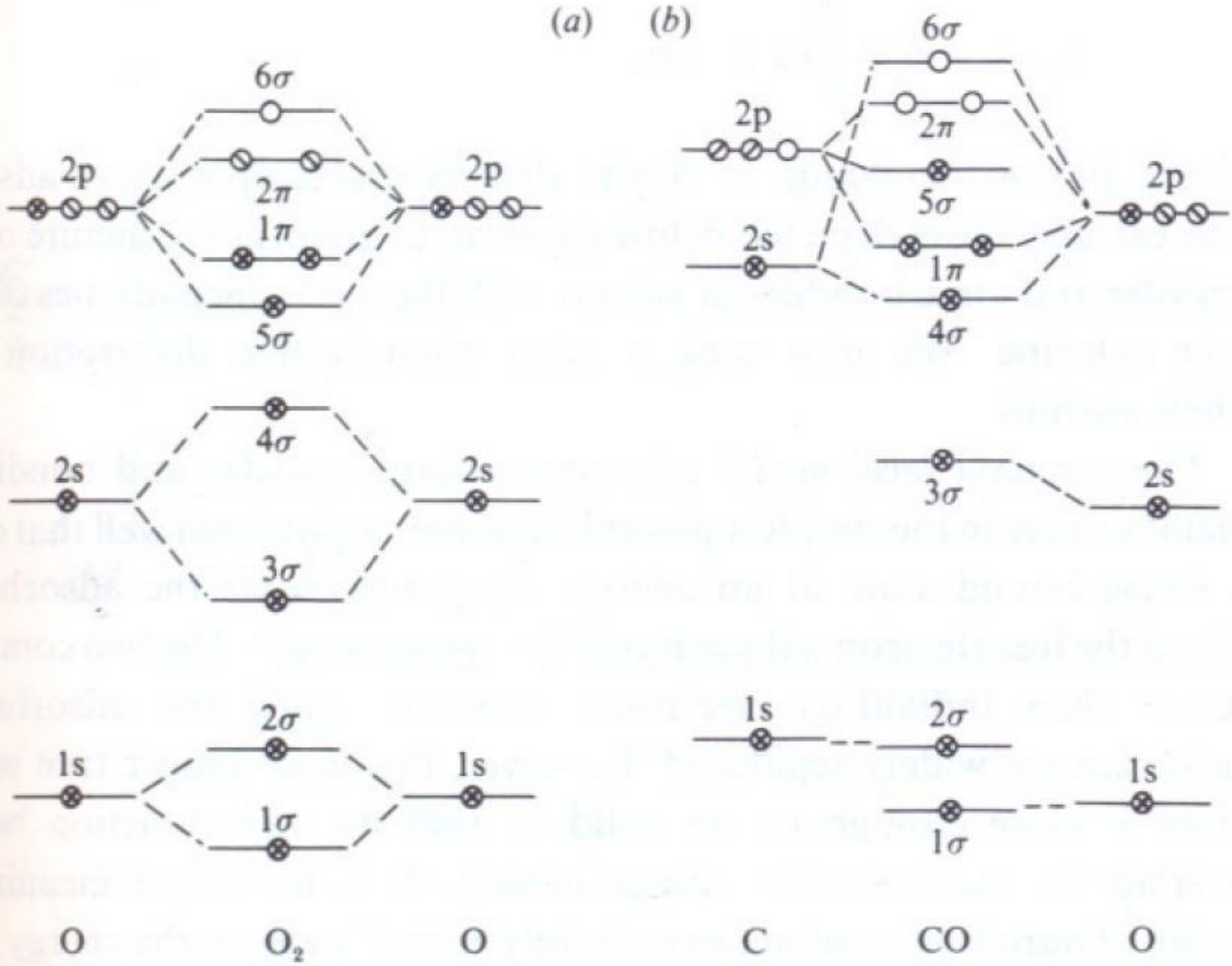

Fig. 9.8. Schematic potential energy and electronic energy level diagram for an adsorbate/substrate complex. The adsorbate local density of states is indicated by a dashed line for both large and small separation distances (Gadzuk, 1974).

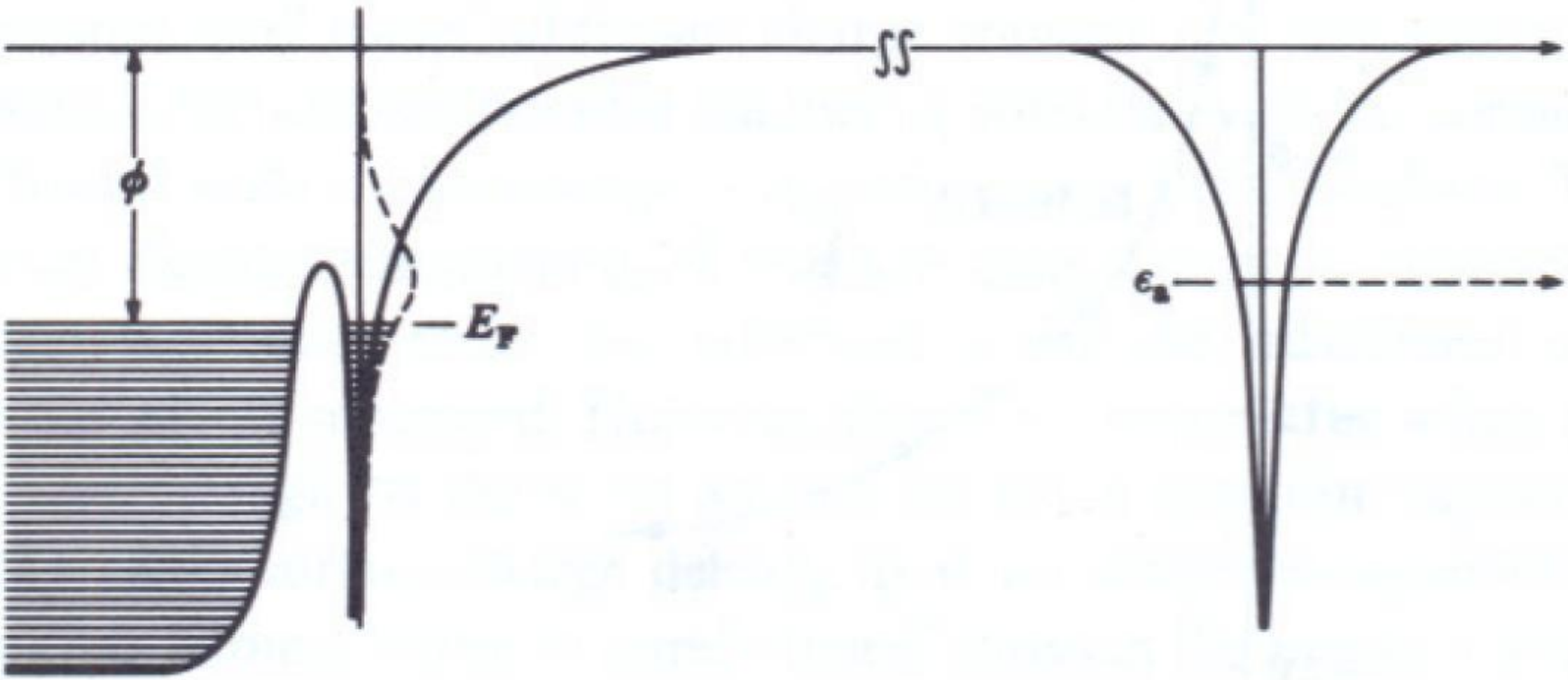

Fig. 2.6

Fig. 9.10. Change in density of states due to chemisorption for Cl, Si and Li atoms adsorbed on jellium ($r_s = 2$). The silicon curve exhibits both 3s-derived and 3p-derived resonances (Lang & Williams, 1978).

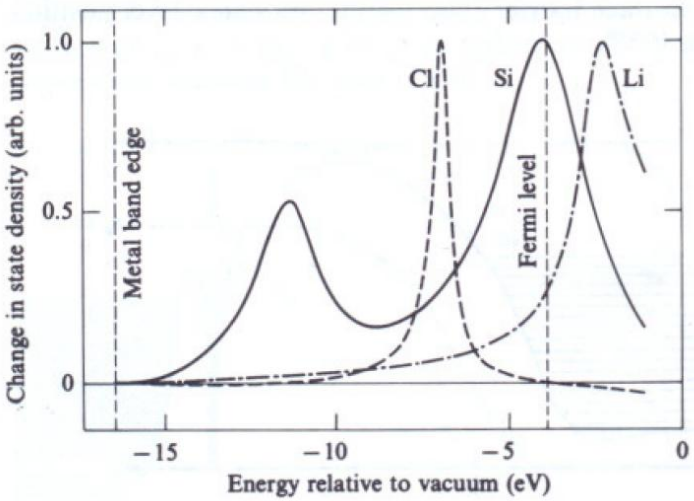

Fig. 9.11. Contours of constant charge density for Cl, Si and Li atoms adsorbed on a jellium substrate: (*a*) total charge; (*b*) induced charge. Solid (dashed) curves denote a surfeit (depletion) of electrons (Lang & Williams, 1978).

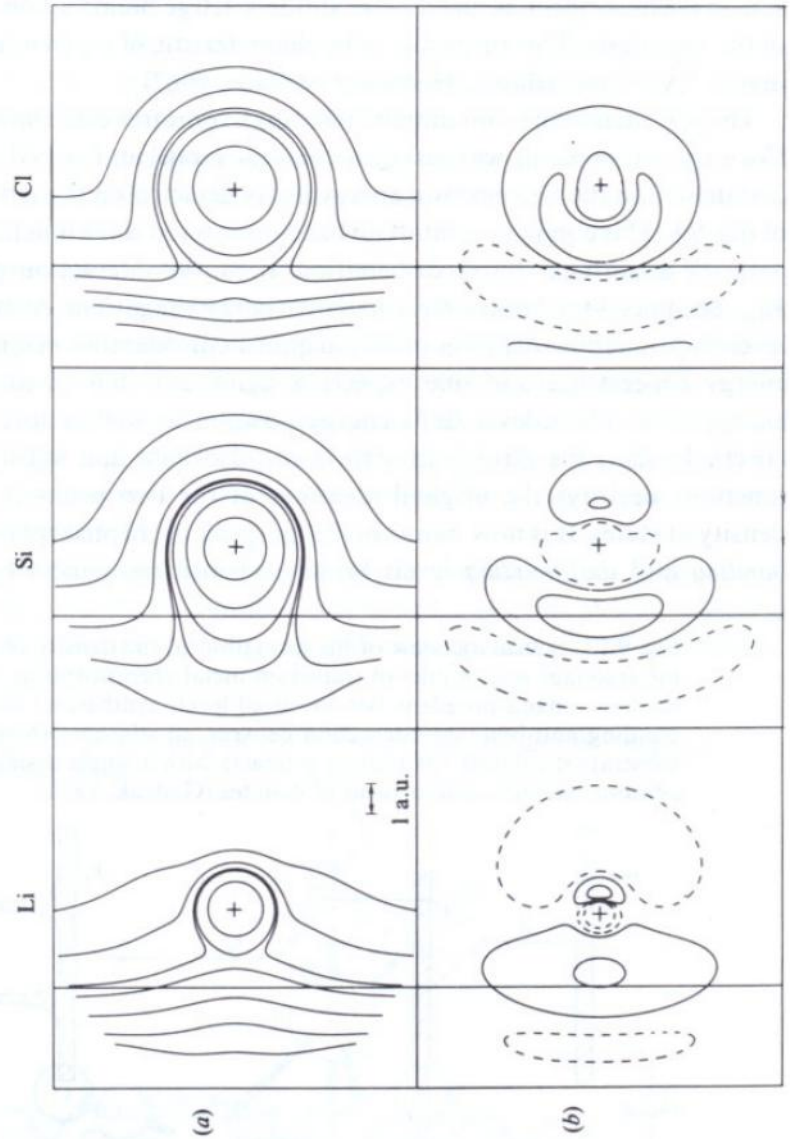

Fig. 2.7

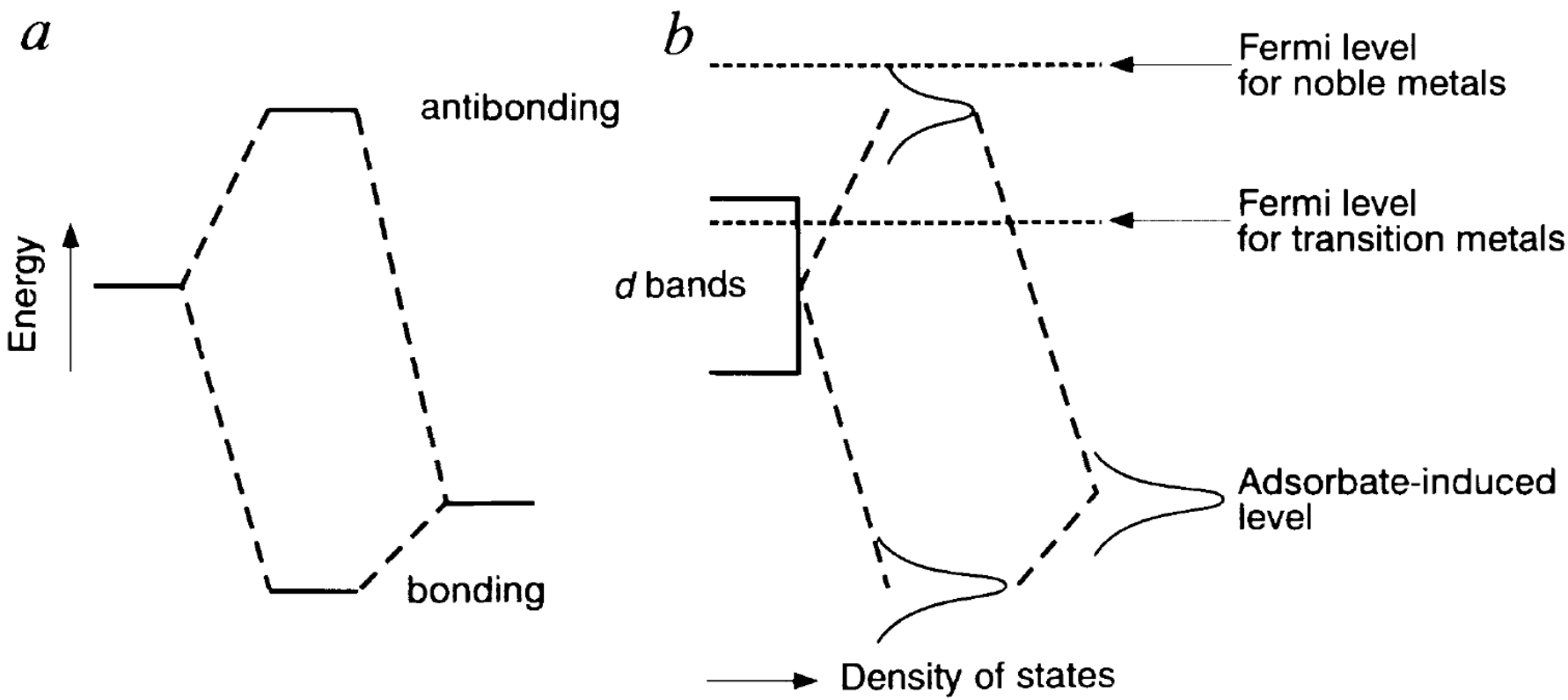
a
antibonding
Energy
bonding
b
Fermi level
for noble metals
Fermi level
for transition metals
d bands
Adsorbate-induced
level
Density of states

Fig. 2.8.

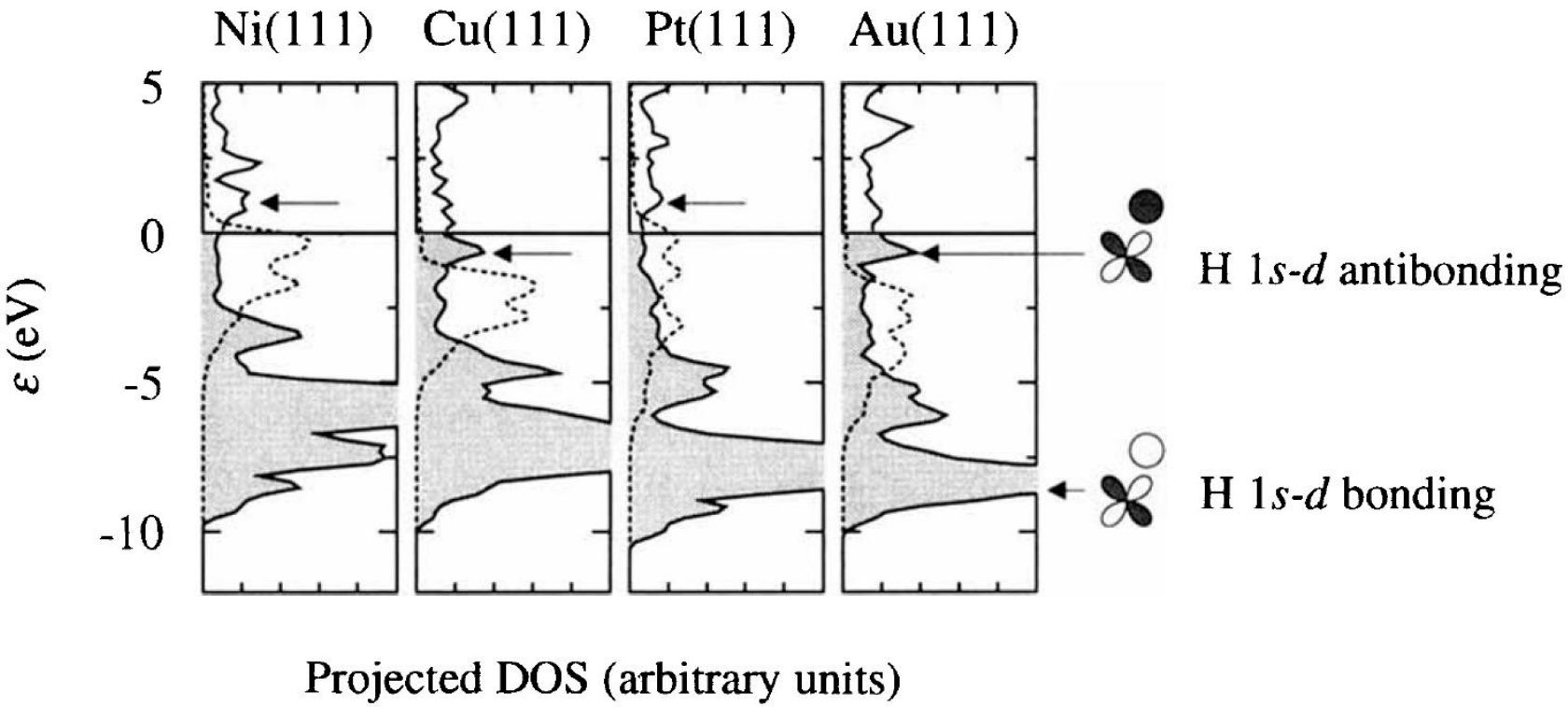
Ni(111)
Cu(111)
Pt(111)
Au(111)
5
0
-5
-10
ε (eV)
H 1s-d antibonding
H 1s-d bonding
Projected DOS (arbitrary units)

Fig. 2.9.

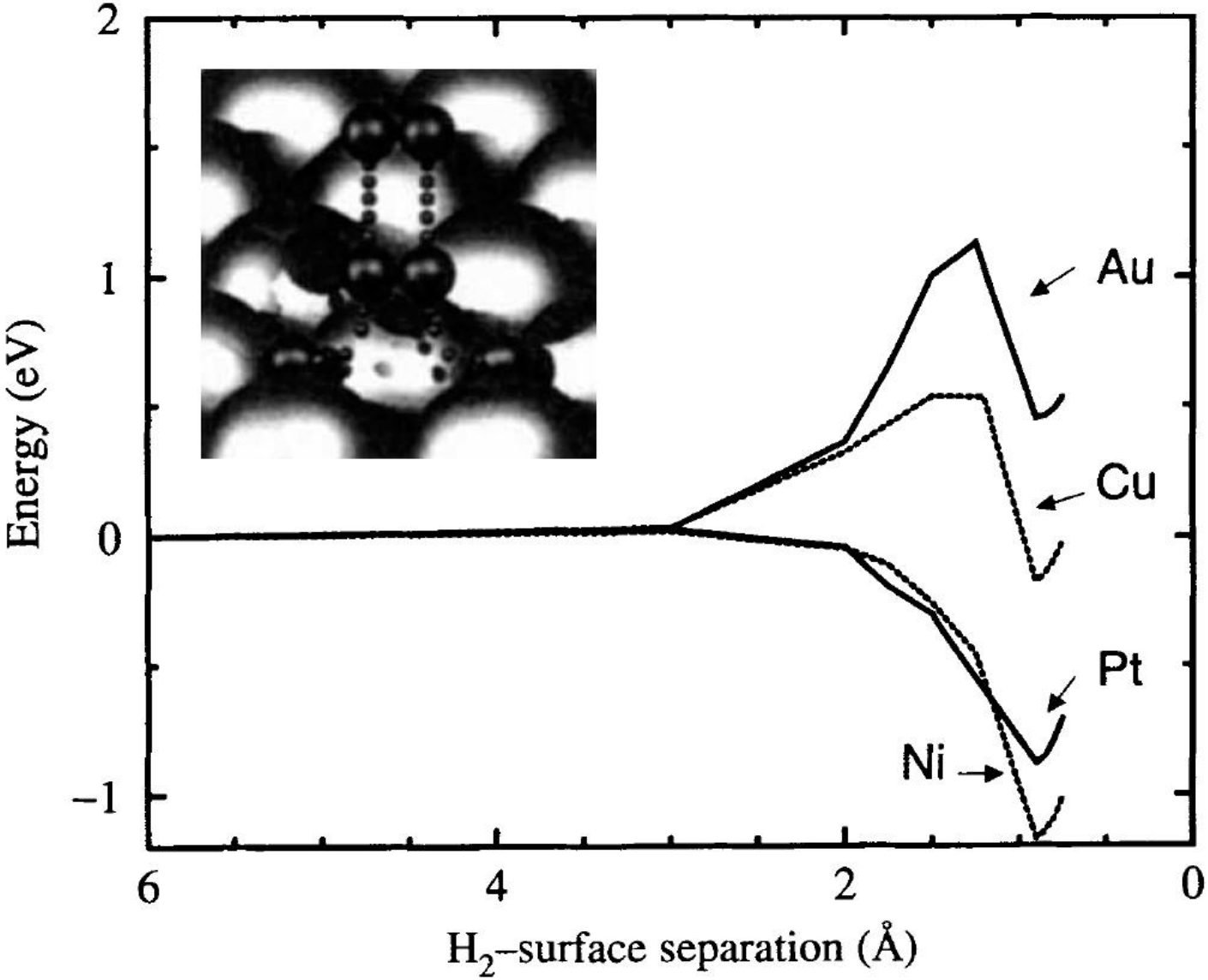

Fig. 2.10

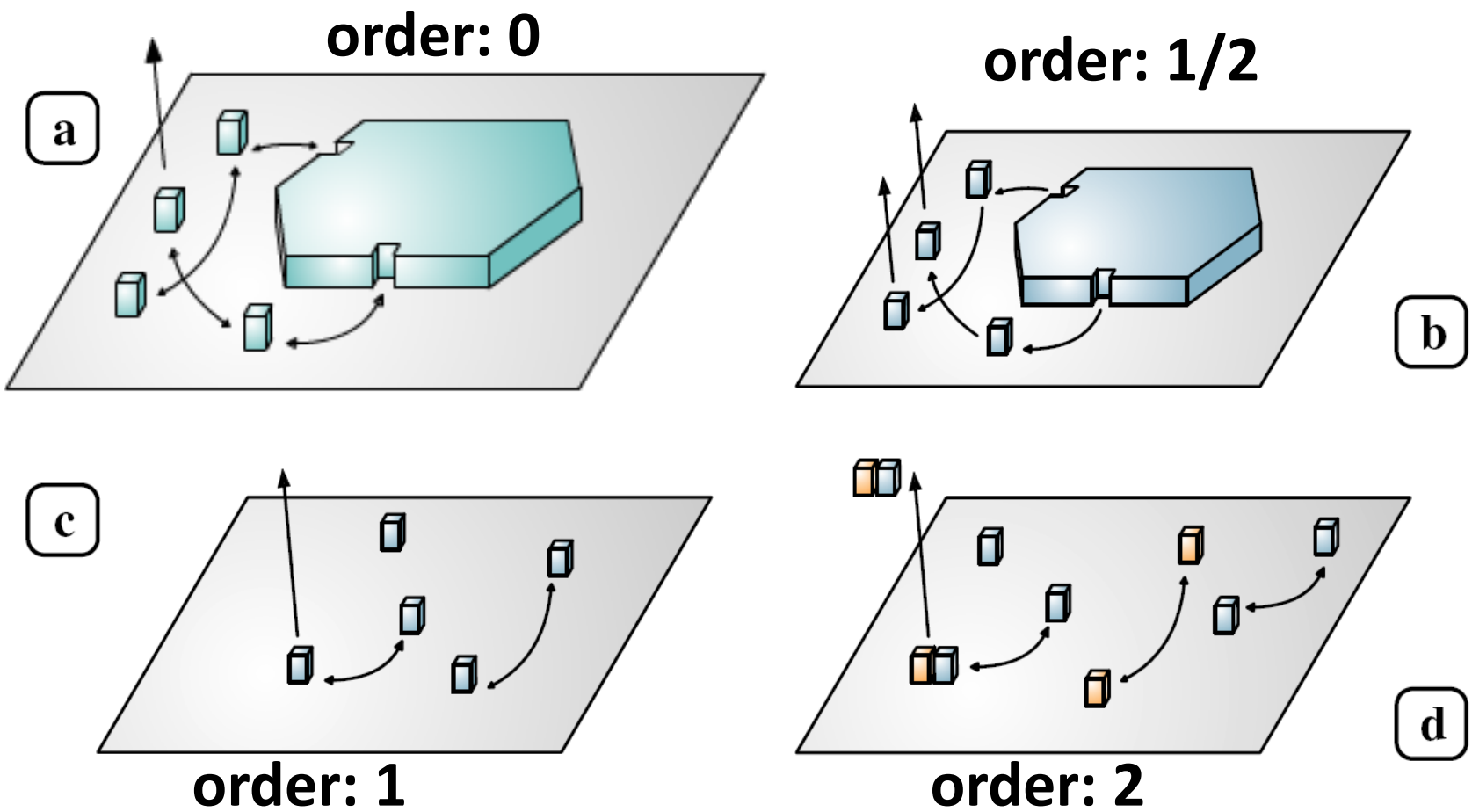

Abb. 2.5: Skizzierung der Ordnungskinetiken: Desorption dicker Filme (a), von Inselrändern (b), mobiler und immobiler Adsorbate (c) und rekombinierter dissoziierter Produkte (d) – Substrat in grau, Adsorbate in türkis und orange

Fig. 2.11.

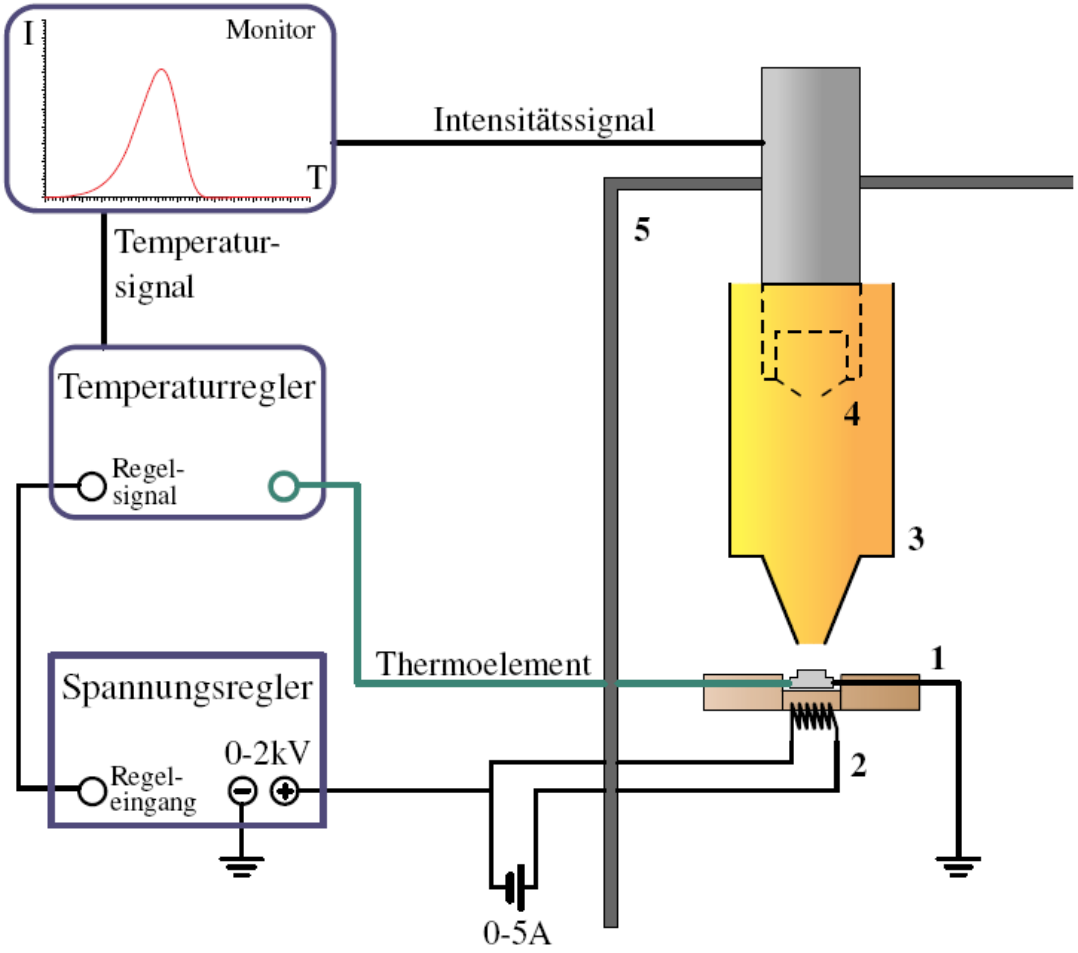

Abb. 3.3: Der Aufbau zur Thermodesorptionsspektroskopie — Probenhalter mit geerdeter und zuvor begaster Probe (1), Wolfram-Heizfilament mit max. 5 A bei ca. 6 V (2), vergoldete Kupferblende (3), Ionisationskammer des Massenspektrometers (4), UHV-Kammer (5).

Fig. 2.12

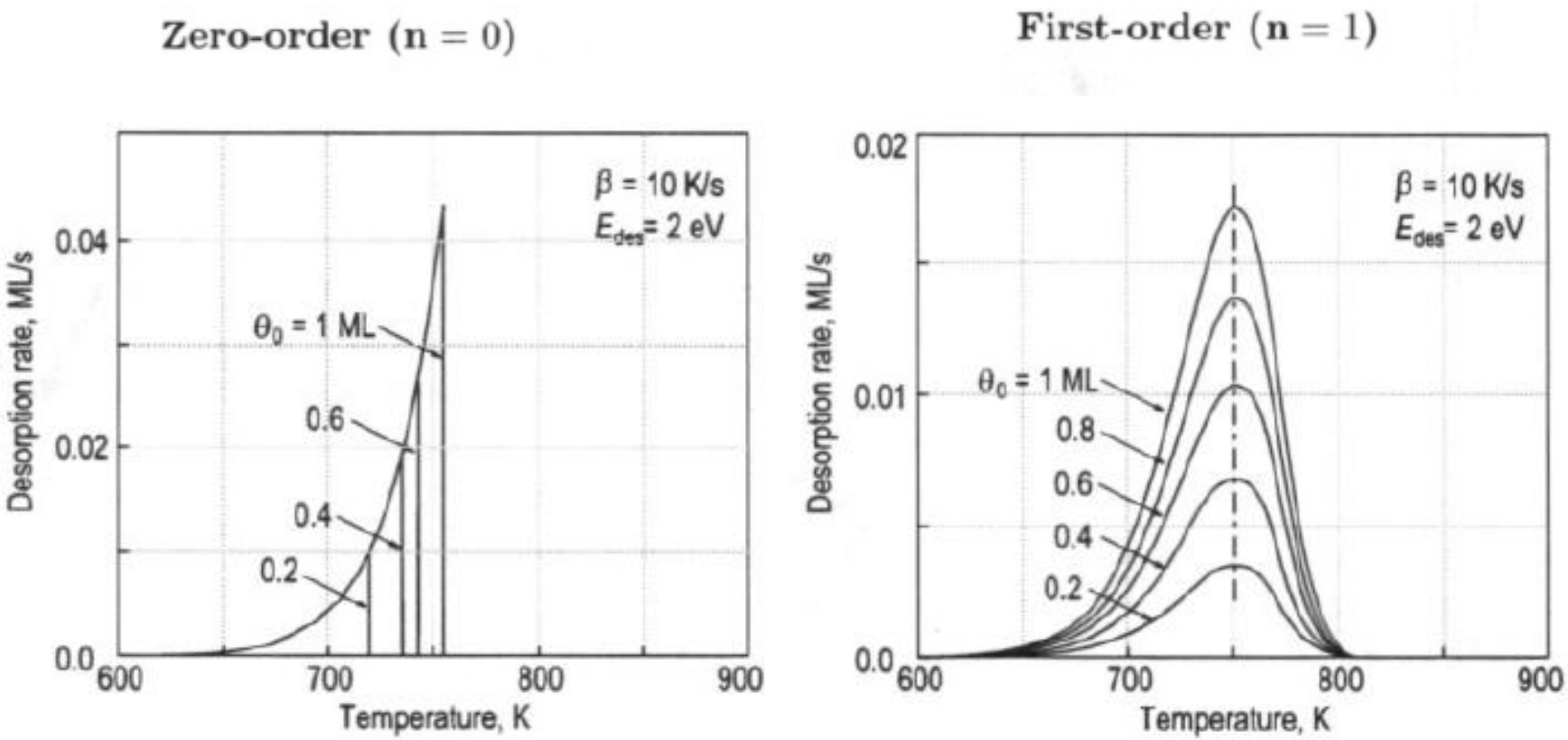
Zero-order (n = 0)
First-order (n = 1)
β = 10 K/s
E_{des} = 2 eV
θ_0 = 1 ML
0.6
0.4
0.2
0.8
Desorption rate, ML/s
Temperature, K
0.0
0.01
0.02
0.04
600
700
800
900

Fig. 2.13

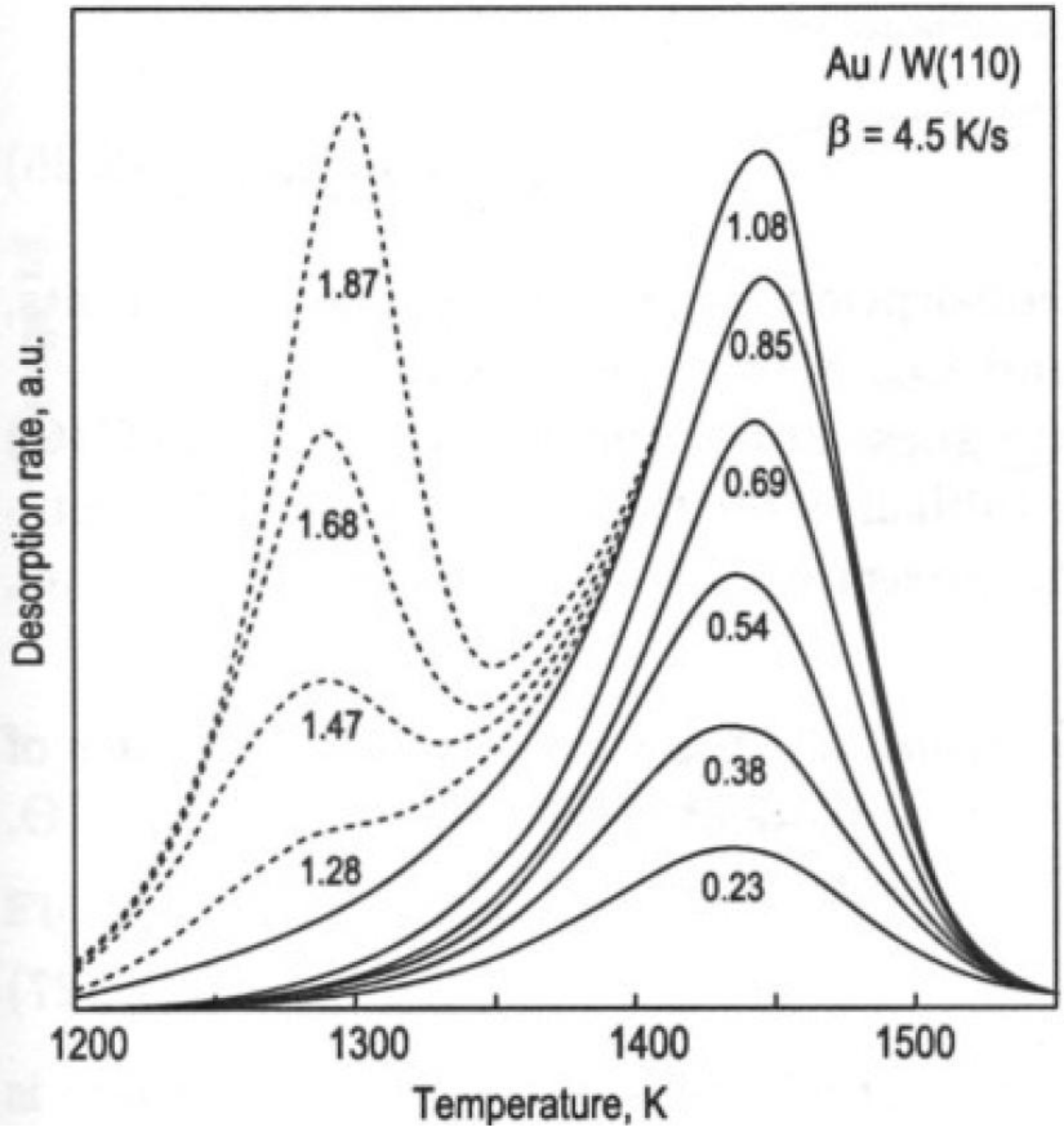
Au / W(110)
β = 4.5 K/s
1.87
1.68
1.47
1.28
1.08
0.85
0.69
0.54
0.38
0.23
Desorption rate, a.u.
1200
1300
1400
1500
Temperature, K

Fig. 2.14

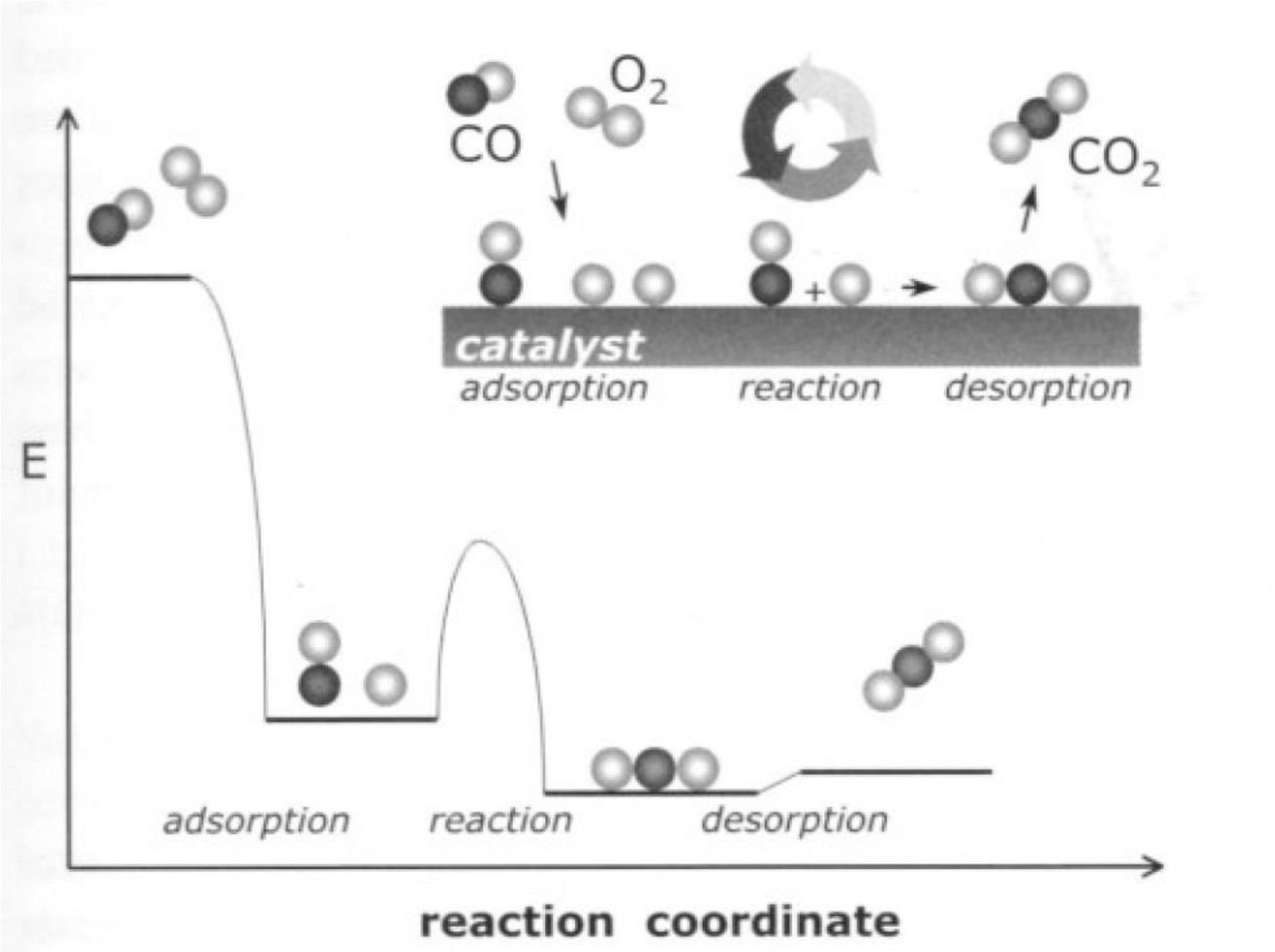

Figure 1.5. Reaction cycle and potential energy diagram for the catalytic oxidation of CO by O_2.

Fig. 2.15

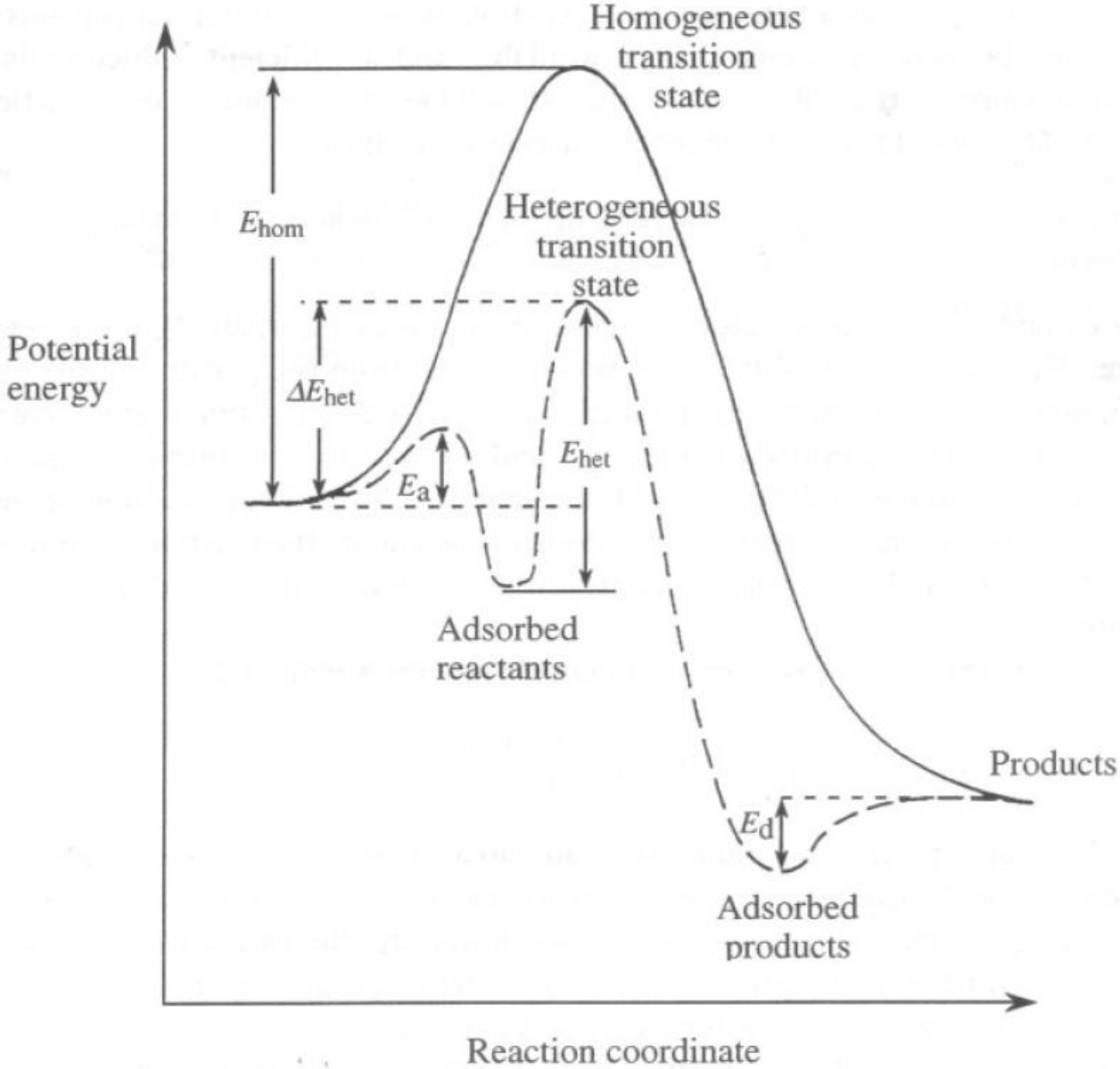

Fig. 4.1 A potential energy diagram, using transition state theory to compare the homogeneous and heterogeneous reaction pathways. (Solid lines indicate the homogeneous process and dashed lines show the heterogeneous process.)

Fig. 2.16

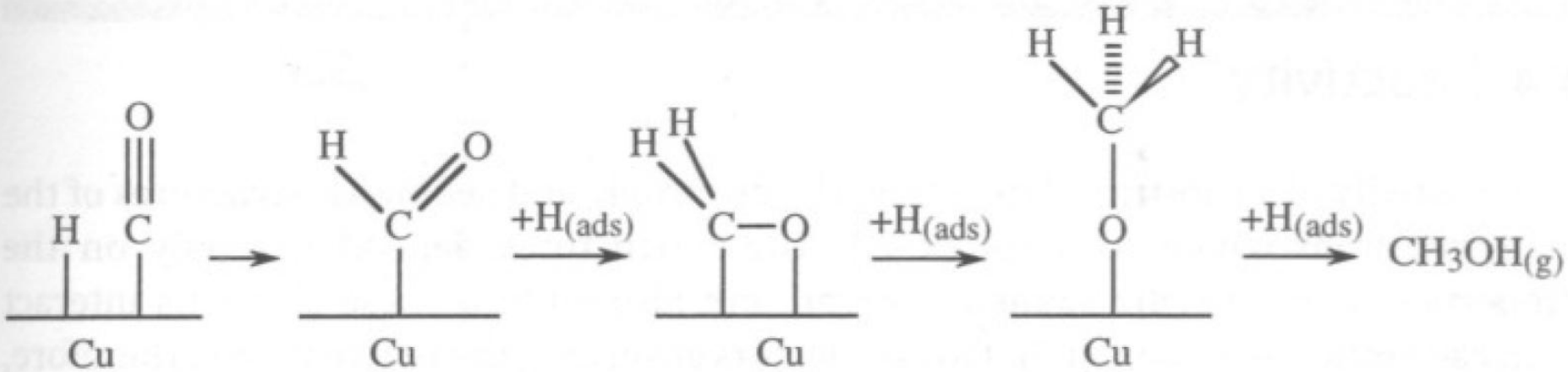

Fig. 4.4 Schematic diagram of the generally accepted mechanism for methanol synthesis from synthesis gas over a copper-based catalyst.

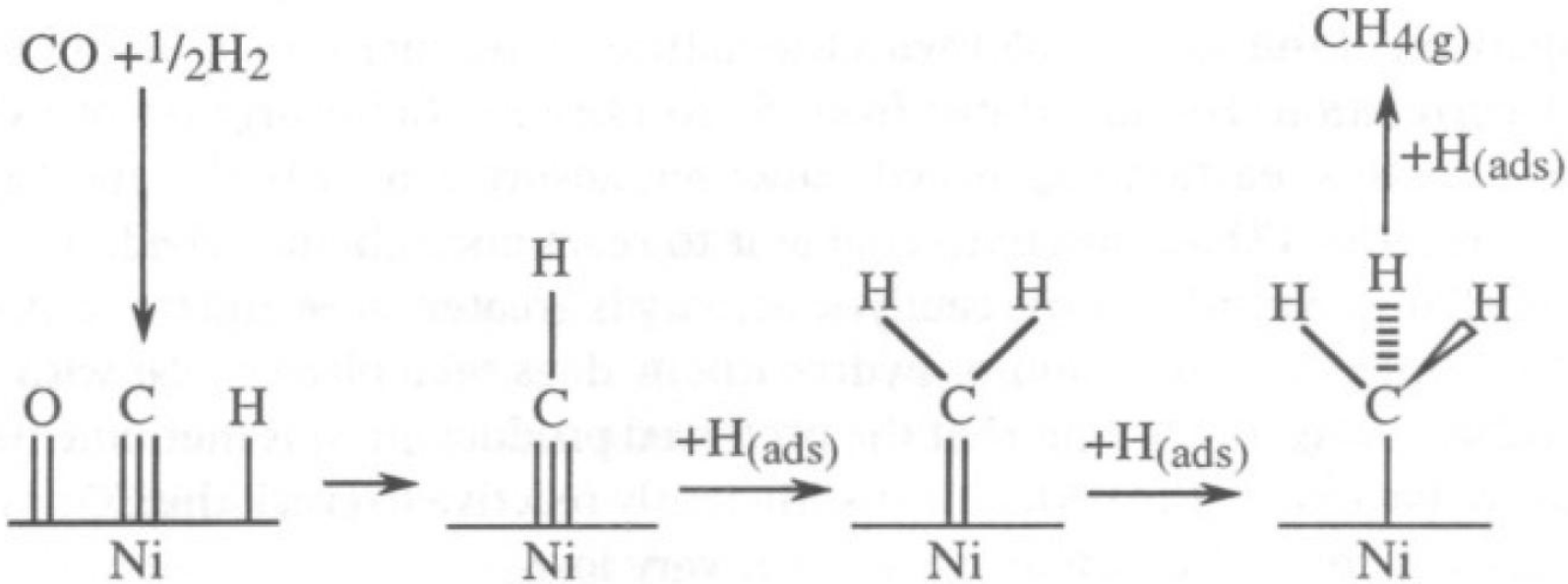

Fig. 4.5 The generally accepted reaction pathway for the methanation reaction of synthesis gas by a nickel-based catalyst.

Fig. 2.17

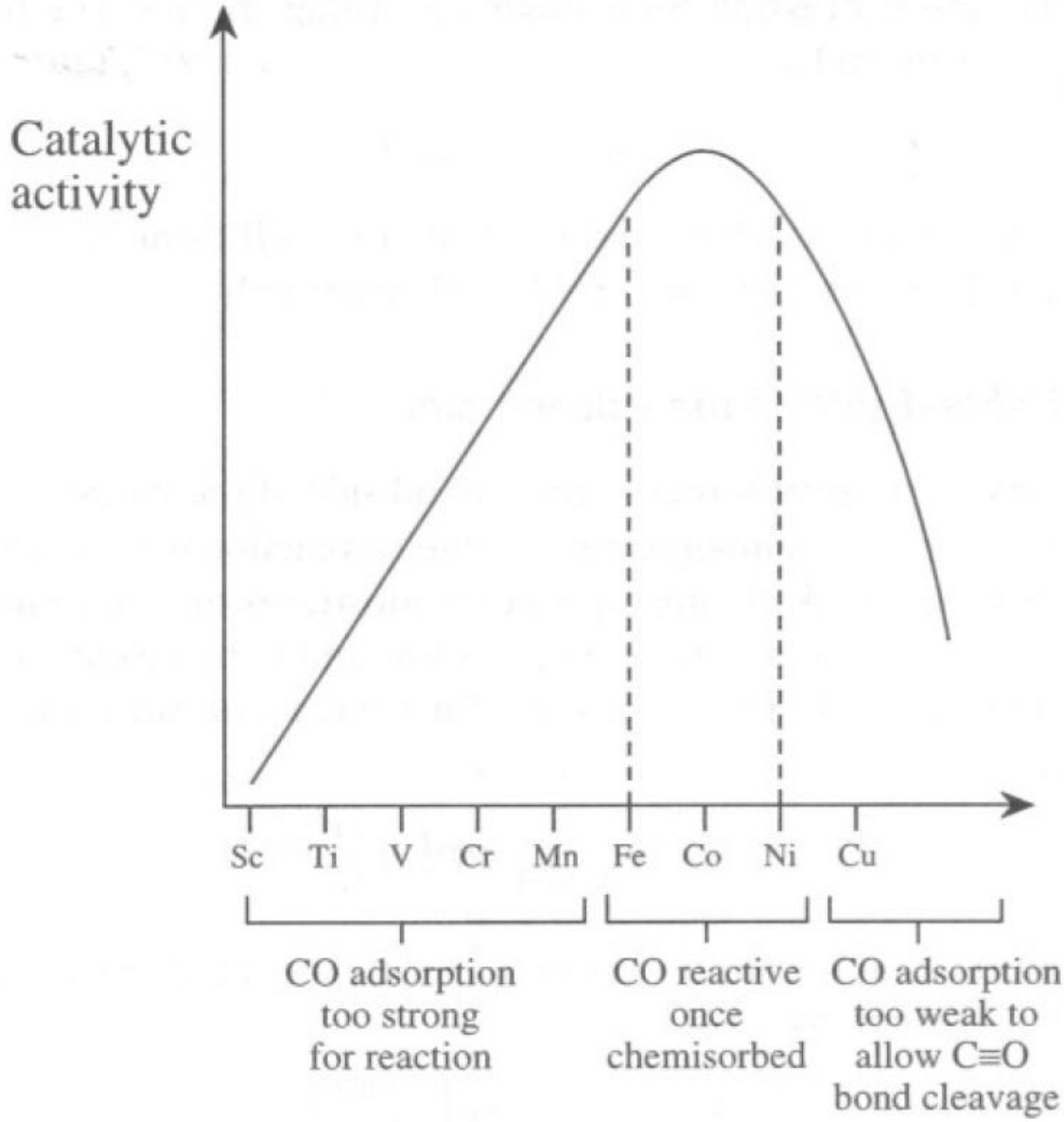

Fig. 4.6 A typical 'volcano plot'; in this case for the Fisher-Tröpsch synthesis of hydrocarbons from synthesis gas, with a correlation to the bonding of CO on the metals.

Fig. 2.18.

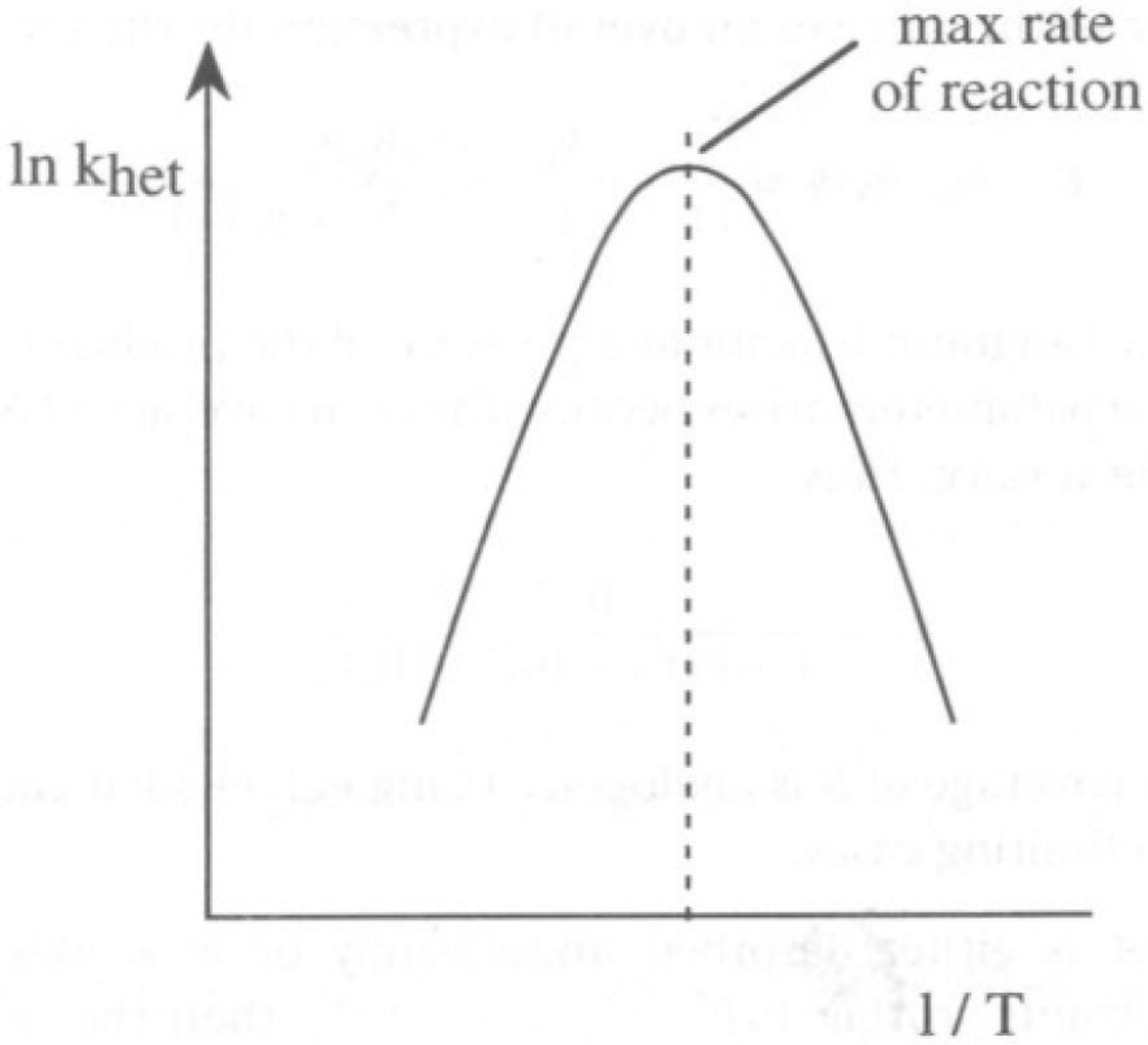

Fig. 4.7 The Arrhenius plot of ln k_{het} versus $1/T$ for a typical surface reaction.

Fig. 2.19

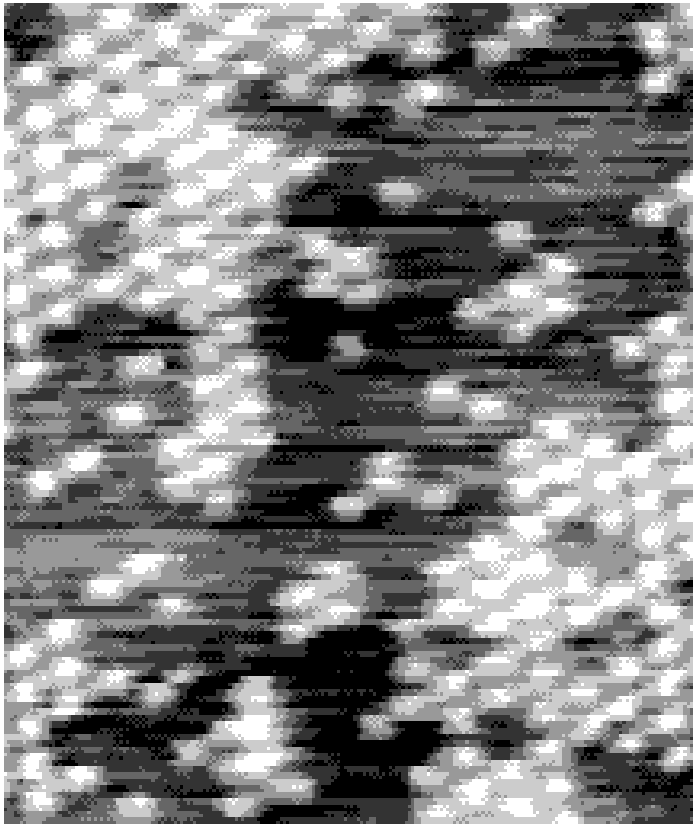

STM movie of O / Ru(0001)
(http://w3.rz-berlin.mpg.de/pc/ERTL/Galerie_E/Ertl_galerie.html)

Fig. 2.21

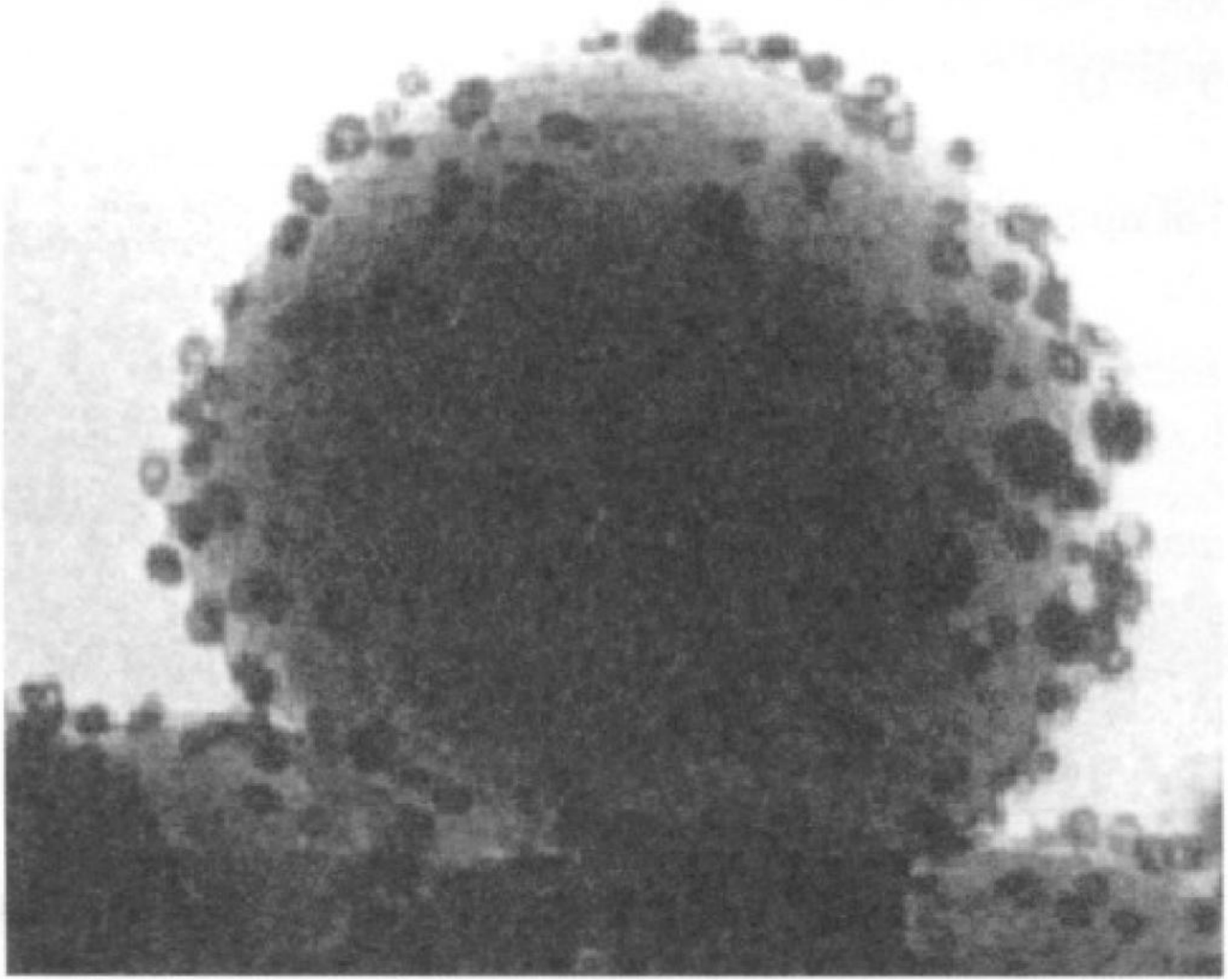

Fig. 2.22.